

SITA: Single Image Test-time Adaptation

Ansh Khurana¹, Sujoy Paul¹, Piyush Rai^{1,2}, Soma Biswas³, Gaurav Aggarwal¹
¹Google Research, ²IIT Kanpur, ³IISc Bangalore

Abstract

In Test-time Adaptation (TTA), given a model trained on some source data, the goal is to adapt it to make better predictions for test instances from a different distribution. Crucially, TTA assumes no access to the source data or even any additional labeled/unlabeled samples from the target distribution to finetune the source model. In this work, we consider TTA in a more pragmatic setting which we refer to as SITA (Single Image Test-time Adaptation). Here, when making each prediction, the model has access only to the given single test instance, rather than a batch of instances, as has typically been considered in the literature. This is motivated by the realistic scenarios where inference is needed in an on-demand fashion that may not be delayed to “batch-ify” incoming requests or the inference is happening on an edge device (like mobile phone) where there is no scope for batching. The entire adaptation process in SITA should be extremely fast as it happens at inference time. To address this, we propose a novel approach AugBN for the SITA setting that requires only forward propagation. The approach can adapt any off-the-shelf trained model to individual test instances for both classification and segmentation tasks. AugBN estimates normalisation statistics of the unseen test distribution from the given test image using only one forward pass with label-preserving transformations. Since AugBN does not involve any back-propagation, it is significantly faster compared to other recent methods. To the best of our knowledge, this is the first work that addresses this hard adaptation problem using only a single test image. Despite being very simple, our framework is able to achieve significant performance gains compared to directly applying the source model on the target instances, as reflected in our extensive experiments and ablation studies.

1. Introduction

Deep neural networks work remarkably well on a variety of applications, specifically when the test samples are drawn from the same distribution as the training data. The performance falls drastically when there is a non-trivial shift between the train and test distributions [7, 22]. In several

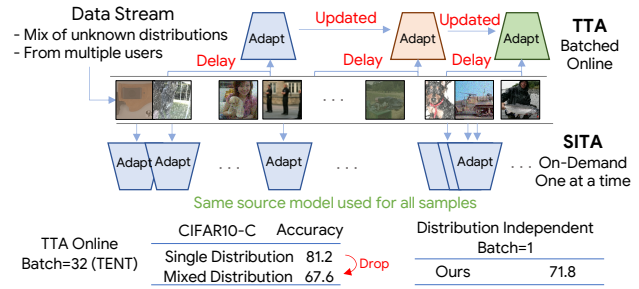


Figure 1. **SITA: Single Image Test-time Adaptation.** SITA is a more realistic version of test-time adaptation setting. The model only has access to the given test instance, rather than a batch of instances. SITA is particularly useful where *batching* may not be feasible due to privacy and/or latency reasons. Online methods with large batch sizes only work well when encountering test data from a single distribution at a time, and suffer a considerable drop in performance when images from multiple different distributions are mixed together and sent as a stream. On the other hand, in SITA, since adaptation is done for each individual test sample independently, it does not suffer from this problem.

real-world settings, such a performance drop may make the model unusable. There have been recent works in the literature to train robust models [9, 21, 26]. While this is a viable research direction for the problem at hand, it entails modifying the training process. This may not always be practical as the training data may no longer be available due to privacy/storage concerns. All that is available is a previously trained model. Therefore, there is a growing interest in *Test Time Adaptation* (TTA), where the models can be adapted at test time, without changing the training process or requiring access to the original training data.

TTT [29] and TENT [30] are among recent works that have been very effective in adapting models at prediction time. TTT [29] uses auxiliary self-supervised tasks to train the source model. The model is then fine-tuned (via the self-supervised sub-network) for every test instance for multiple iterations. Using TTT for adapting a new model, one needs to modify the training process (adding self-supervised sub-network) and hence needs access to the source training data, which may not be always available. Further, the multiple backward passes take considerable amount of time

Table 1. Characteristics of various problem settings that deal with adapting a model (trained on a source distribution) to a test distribution. We propose SITA (Single Image Test-time Adaptation), which is the hardest adaptation setting.

Setting	Source Data	Target Label (y^t)	Train Loss	Test Loss	Offline	Online Statistics	Batched
fine-tuning	-	✓	$\mathcal{L}(x^t, y^t)$	-	✓	-	✓
domain adaptation	x^s, y^s	✗	$\mathcal{L}(x^s, y^s) + \mathcal{L}(x^t, x^s)$	-	✓	-	✓
source free domain adaptation	✗	✗	$\mathcal{L}(x^t)$	-	✓	-	✓
test-time training [29]	x^s, y^s	✗	$\mathcal{L}(x^s, y^s) + \mathcal{L}(x^s)$	$\mathcal{L}(x^t)$	✗	✓	✓
fully test time adaptation [30]	✗	✗	✗	$\mathcal{L}(x^t)$	✗	✓	✓
SITA	✗	✗	✗	✗	✗	✗	✗

which may not be available where latency is not acceptable. TENT [30], on the other hand, adapts the given trained model, without accessing the source data. TENT assumes that the data comes in batches, with batch size usually much greater than one. It considers an online setting, where the model adapted to the current instances (batch) is used for adapting the subsequent instances (batches), which implies that the model has information about all the test instances seen till a certain point. Motivated by the success and limitations of TTT [29] and TENT [30], we enumerate the following desirable properties of algorithms developed for the realistic, and challenging SITA protocol

- Do not require access to the source training data.
- Almost as fast as the original model.
- Can adapt to a single test instance and does not require batching.
- Model adapted to one test instance should not be used for the subsequent instances.

The first property is not only related to privacy/storage issues, but also speed, as any re-training on the source data would make the approach much slower. The motivation behind the third property is latency and privacy. For large batch sizes, one has to wait for a certain number of samples, leading to delays, or club samples from multiple users, which may have privacy concerns. The last property is motivated by the fact that different test instances/batches may come from very different distributions, which will adversely affect the performance of the model. Figure 1 compares the SITA setting with other TTA settings in literature. Online methods which use large batch sizes, like TENT [30], improve performance by evaluating one corruption type at a time (single distribution), and resetting the model for the next corruption type. When evaluated by shuffling all 15 corruption types in the CIFAR-10-C [8] dataset (mixed distribution), their performance drops considerably, as shown in Figure 1.

In this work, we propose a novel approach, termed **AugBN**, which has all the above properties of the Single Image Test-time Adaptation (SITA) setting. The proposed method does not assume any access to the source data, adapts to one test instance at a time, and resets the model to the given source model for adapting to every new test instance.

The core of our method lies in calibrating the batch-norm statistics of the network. Instead of using the source batch-norm statistics for testing, we calibrate it using the statistics from the individual test instances. However, as estimating them from a single test instance is unreliable, we utilize certain augmentations of the test instance for this task. Our adaptation method uses only one forward pass and thus is quite fast (comparable to using the source model directly), unlike TENT [30] and TTT [29], which require at least one backward pass. The main contributions of this work are summarised as follows:

1. We formalise the pragmatic **Single Image Test-time Adaptation (SITA)** setting.
2. We propose AugBN that performs fast adaptation in both dense and sparse prediction tasks, with only one forward pass.
3. We achieve state-of-the-art performance for SITA on both classification and segmentation tasks.

2. Related Work

Table 1 summarizes the characteristics of various settings which adapt a model trained on a *source* distribution to a *target* distribution. Fine-tuning and domain adaptation are offline methods, that is, they assume access to the entire source and target dataset to adapt and thus are out of scope for *test time* settings. We divide the discussion on related works based on the characteristics of the *test time* setting proposed by recent works.

Source-free Domain Adaptation. One of the constraints of SITA is that we cannot use the source data while adapting, but only use the trained source model. Recent works in literature tackle this problem, but using an unlabeled target set for adaptation, with the hypothesis that the test instances are drawn from the target distribution. These methods involve - entropy minimization with divergence maximization [15], pseudo-labeling with self-reconstruction [32], as well as generating additional target images [13, 16] and robustness to dropout [25]. Unlike these methods, in SITA, we do not have any target set to adapt and do not have any assumption over the distribution of the test instances.

Test Time Training. In this setting, self-supervised tasks are introduced during training of the source models. These self-supervised tasks are later used at test time, allowing adaptation of the shared encoder between the main prediction branch and the auxiliary self-supervised task branch. TTT [29], one of the first works to formalize test time training, uses the self-supervised task of rotation prediction. Karani *et al.* [12] proposed test time adaptation for medical image segmentation where instead of training an auxiliary branch, they trained a denoising autoencoder on the label space, and used its error as a self-supervised loss at test time. Other recent works [1] extend the auxiliary branch based approach by using meta-learning to ensure that test-time training on the auxiliary branch would improve predictions from the main branch. These approaches cannot utilise any off-the-shelf model and improve its performance at test time. Instead they need to re-train the source model with hand-crafted and often complicated training strategies.

Fully Test Time Adaptation. These approaches have the advantage of adapting off-the-shelf models, since they do not rely on any auxiliary task. The state-of-the-art method in this category, TENT [30], formalised this setting and achieved better performance than some of the methods which actually re-train the source model. TENT runs an online optimization over a given test set, which minimizes the entropy of the predicted distribution for every incoming batch. Although the method can be made to work in the SITA setting where the model is reset after every test instance, their results are primarily focused in the online setting by gradually adapting the model over the test set. It gives impressive performance in the online setting, but we observe significant drop in performance in the SITA setting (Figure 6c), when there is only a single test instance. [19] improves upon TENT by adjusting the loss function to a log-likelihood ratio instead of entropy, and maintaining a running estimate of the output distribution. This setting, while clearly more useful than the previous one, is not as realistic as SITA because it needs to (i) accumulate and store samples to create batches, (ii) run an online optimisation under the assumption that the test samples come from the same distribution.

BatchNorm Adaptation. Recent literature on domain-adaptation proposes adapting the statistics of only the Batch Normalization layers for adjusting to the test distribution. Though these works are not targeted towards the TTA task, they suggest that adapting normalization statistics could provide significant performance gains, without requiring hand-crafted loss functions. Prediction Time Normalization (PTN) [20] uses the mean and variance of the current test batch as the statistics in the batch norm layer, instead of using the accumulated statistics of the source data. This works reasonably well if the test batch size is large enough to provide a good estimate. Schneider *et al.* [27] use a similar

approach with focus on improving robustness to corruption. The source model’s accumulated statistics are combined with statistics accumulated over all the available test images to reach a reliable estimate. They show usefulness of the approach in two settings: (i) *full adapt* where the entire test set is available for offline adaptation and (ii) *partial adapt* where a subset of the test set is available for offline adaptation. A special case of the *partial adapt* setting, where only one image is available at a time can be considered as test time adaptation. While Schneider *et al.* [27] do not report results on test time adaptation, they provide suggested hyper-parameter values when only one image is available. Thus, we include this method as a relevant baseline. Our AugBN algorithm is similar in spirit to these works, designed specifically to provide a reliable batch norm statistics estimate at test time, within the constraints of the proposed SITA setting. Our method improves test time statistics estimation by including augmented samples around the current test image.

3. Methodology

We next discuss in detail the SITA setting and propose a simple, yet effective solution for the same. We first formally define the problem statement, and then discuss the challenges that motivate our proposed approach.

3.1. Problem Statement

Consider that we have a model $f_\theta : \mathbf{x} \rightarrow \mathbf{y}$, which is trained on a dataset, which we will refer to as the *source*. This model may not perform well on test data drawn from distributions other than the source, which can be either a corrupted version of the source itself or images drawn from a different distribution, both of which will be referred to as the *target*. The goal is to adapt the model f_θ such that the adapted model performs better on the target images compared to directly using the source model. As motivated in Section 1, we focus on the challenging SITA setting, where inference has to be done on a single image at a time, and not a batch of instances, with the model being reset to the source model after every test instance adaptation. The setting can apply to both sparse and dense prediction tasks.

3.2. Internal Covariate Shift

In deep neural networks, the mean and covariance statistics of every batch-normalization layer are learned using exponential moving average during training, and these accumulated statistics are usually used during testing, as given below for a particular layer:

$$\text{BN}(\mathbf{F}) = \gamma \frac{\mathbf{F} - \mathbb{E}_s[\mathbf{F}]}{\sqrt{\text{Var}_s[\mathbf{F}]}} + \beta \quad (1)$$

where \mathbf{F} is the input feature to the batch norm layer and γ, β are scale and shift parameters, also learned during training.

The subscript s indicates source data. The underlying reason behind using the train statistics instead of the test batch statistics is that the train statistics are estimated on a much larger set compared to a batch of test data, which is much smaller and hence can give a biased estimate of the statistics. While this method works well for the test samples drawn from a distribution similar to the source, its performance may degrade if the test samples come from a different distribution. This is because the feature distribution F of the intermediate layers of the network may have mean and variance shifted from the train statistics, due to the shift in the input distribution. This is often termed as internal covariate shift [11, 27].

To mitigate this problem, the statistics can be estimated from the target dataset and used instead of the learned source statistics, i.e., replace $\mathbb{E}_s[F]$ and $\text{Var}_s[F]$ in Eqn. (1) with $\mathbb{E}_t[F]$ and $\text{Var}_t[F]$, which can be computed as follows:

$$\begin{aligned}\mathbb{E}_t[F] &= \frac{1}{n_t H W} \sum_{i,j,k} F_{i,j,k} \\ \text{Var}_t[F] &= \frac{1}{n_t H W} \sum_{i,j,k} (F_{i,j,k} - \mathbb{E}_t[F])^2\end{aligned}\quad (2)$$

$F_i \in \mathbb{R}^{H,W,F}$ is the feature map of the i^{th} instance. H, W, F are the height, width and feature dimension respectively. $j \in \{1, \dots, W\}$, $k \in \{1, \dots, H\}$ and n_t is the number of target instances in the dataset. This is exactly what is done in several recent domain adaptation works [2, 14], where we have access to a *target training set* on which we can estimate distribution statistics. However, in our setting, we do not have access to such a train set from the target distribution. In fact, we need to adapt to one test instance at a time, and cannot use the updated model or the current instance's statistics to infer the subsequent test instances. This makes our setting much harder compared to other settings in literature on test time adaptation [30].

3.3. Single Image Statistics Estimation

Given a single test instance, we can estimate its statistics (μ_t, σ_t) using Eqn. (2), with $n_t = 1$. However, this estimate may be unreliable as it is computed using a single instance. To address this, instead of replacing the source statistics in Eqn. (1) with the single test image statistics, we can obtain a more reliable estimate for every batch-norm layer as follows:

$$\begin{aligned}\mu &= \lambda \mathbb{E}_s[F] + (1 - \lambda) \mu_t \\ \sigma^2 &= \lambda \text{Var}_s[F] + (1 - \lambda) \sigma_t^2\end{aligned}\quad (3)$$

where $\lambda \in [0, 1]$. This strategy considers the source statistics as a prior. On one hand, $\lambda = 1$ results in using the source model directly on the target test instances. In this case, the estimator has high bias. On the other hand, $\lambda = 0$ results in using only the single test image statistics. In this case, the variance of the estimator is high. The estimator in Eqn. (3)

provides a balance to bias and variance, with the underlying hypothesis that the target distribution is a shifted version of the source. It can be shown that the mean estimator has $(1 - \lambda)^2$ times lower variance and $||(1 - \lambda)(\mathbb{E}_s[F] - \mathbb{E}_t[F])||$ lower bias magnitude than the worst variance and bias of the two estimators corresponding to $\lambda = 1$ and $\lambda = 0$.

3.4. Augmentation for Statistics Estimation

Ideally, we want the single image estimate of μ_t, σ_t to be as close as possible to the true mean and variance of the target distribution. The variance of the above estimators can be reduced by increasing the number of samples. Given that we have only one sample x at hand, we ask the question - *is it possible to generate more data points to improve the estimates?* While we do not have access to the underlying distribution of the target instances, we can possibly create data points in the vicinity of x . Inspired by the recent works in contrastive learning for representation learning [4] and theoretical justifications of pseudo-labeling [31], which suggests that using neighborhood samples via augmentation helps in the respective tasks, we adopt this idea for our task to improve the estimate of target image statistics.

Specifically, we use a set of augmentations to augment x and obtain $\{\hat{x}_1, \dots, \hat{x}_n\}$. This generates features $\{\hat{F}_1, \dots, \hat{F}_n\}$ for a certain batch normalization layer, and we use these features along with the original feature F to obtain a better estimate of the statistics, μ_t and σ_t from the given single image. However, as it is hard to control the distribution of the augmented samples, and certain augmentations can outweigh the estimation, instead of assigning the same weight to all the augmented samples as the original sample, we distribute the weight as follows:

$$\begin{aligned}\mu_t &= \mathbb{E}_w(\{F, \hat{F}_1, \dots, \hat{F}_n\}; w = \{1/2, 1/2n, \dots, 1/2n\}) \\ \sigma_t &= \text{Var}_w(\{F, \hat{F}_1, \dots, \hat{F}_n\}; w = \{1/2, 1/2n, \dots, 1/2n\})\end{aligned}\quad (4)$$

In our work, we choose a fixed set of augmentations $\{a_1, \dots, a_m\}$, from which we randomly pick $k (\leq m)$ augmentations. These are used to get the augmentation functions A_i , which compose multiple augmentations to generate augmentation images \hat{x}_i . Since these new samples \hat{x}_i are generated from a single parent sample \hat{x} , the samples are not independent. Thus, the variance reduction may not be linear with the number of augmented samples used (as the underlying assumption in that case is that the samples are independent). Having said that, using the augmented samples does improve the performance over a range of tasks, as we observe in our experiments (Section 4). The entire algorithm to adapt the model during prediction is shown in Algorithm 2, which uses the proposed AugBN layer (Algorithm 1). A pictorial representation of our proposed method is presented in Figure 2. We must highlight the simplicity of our method,

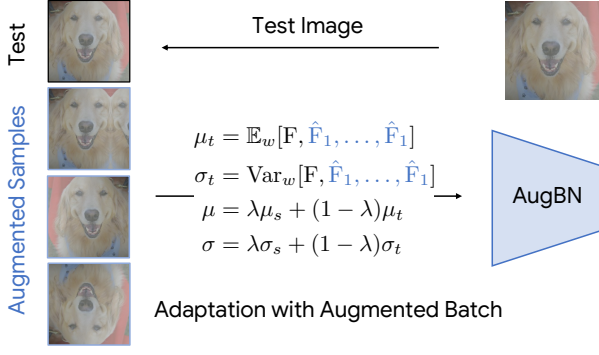


Figure 2. Proposed method (Algorithm 2). The input test image along with a combination of augmented samples are used to estimate the batch-norm statistics using Eqn. 4. This estimation happens with one forward pass through the network defined using our proposed AugBN layer (Algorithm 1)

as it can be easily implemented by just replacing the vanilla BN layers in any network with AugBN.

Algorithm 1: AugBN

Input: - Source statistics: μ_s, σ_s , prior = λ
- Input batch features: $F, \oplus \{\hat{F}_i\}_{i=1}^n$.
Output: Normalised Features:
 $\bar{F} = \text{AugBN}(F, \{\hat{F}_i\}_{i=1}^n)$
 $\ominus \bar{F} \leftarrow \frac{F - \mu_s}{\sigma_s}$
 $\oplus \mu \leftarrow \lambda \mu_s + (1 - \lambda) \mu_t$ (Eqn. 4)
 $\oplus \sigma \leftarrow \lambda \sigma_s + (1 - \lambda) \sigma_t$ (Eqn. 4)
 $\ominus \bar{F} \leftarrow \frac{F - \mu}{\sigma}$

Comment: \oplus and \ominus signify additions and removals from the standard batch normalization layer)

Algorithm 2: Proposed Algorithm for SITA

Input: - Single Image: x
- Source Model: f_θ
Output: Prediction: y
 $\hat{f}_\theta \leftarrow \text{Repalce BN Layer in } f_\theta \text{ with AugBN Layer}$
for $i = 1 \dots n$ **do**
 $A_i \leftarrow \text{Compose}(\text{RAND-Choose-}k(\{a_i\}_{i=1}^m))$
 $\hat{x}_i \leftarrow A_i(x)$
end
 $y \leftarrow \hat{f}_\theta(x, \hat{x}_1, \dots, \hat{x}_n)$

Comment: RAND-Choose- $k()$ uniformly randomly chooses $k (< N)$ augmentations from the given set.

4. Experiments

To demonstrate the effectiveness and universality of our adaptation approach, we perform thorough experimentation on a variety of publicly available adaptation datasets for both segmentation and classification tasks. In comparison, the focus of most related works has primarily been on classification tasks.

4.1. Semantic Segmentation

Datasets and Implementation Details. We evaluate our method on three different source \rightarrow target combinations covering not only outdoor scenes, but also indoor scenes, to showcase the wide usability of our algorithm. For outdoor, we evaluate on GTA5 [23] \rightarrow Cityscapes [5] and SYNTHIA [24] \rightarrow Cityscapes. For indoor, we show results on SceneNet [18] \rightarrow SUN [28]. The outdoor and indoor scene datasets have 19 and 13 categories respectively. Refer to Appendix A for more details.

Following the literature on domain adaptation of semantic segmentation models, we use Deeplab-V2 [3] with ResNet-101 [6] as the backbone. We use one GPU to train source models with a batch size of 1 in all experiments. We use SGD with an initial learning rate of 2.5×10^{-4} with polynomial decay of power 0.9 [3]. We use the standard metric of mean intersection over union (mIoU) [3] to evaluate. Note that we use only one augmented image and prior ($\lambda = 0.8$) in all experiments on segmentation, unless otherwise mentioned. We use Gaussian blur and random rotation as augmentations, i.e., with $k = m = 2$ (Algorithm 2).

Baselines. We compare with the strong state-of-the-art baselines, namely TENT [30], BN [27], and Prediction Time Normalization (PTN) [20]. All methods are run in the SITA setting, that is, the test batch size for all experiments is fixed to 1 and no method is allowed to run an online optimization or to maintain online statistics. For TENT, we use one epoch of optimization with a learning rate of 10^{-3} (this is the best result we obtained by experimenting over a range between $[10^{-2}, 10^{-5}]$) with Adam optimizer as it provides the best computation time vs performance trade-off. For BN, we showcase their method with the recommended hyper-parameter setting ($N = 16$) for the single image case.

Comparison with state-of-the-art. Table 2 shows the mean Intersection of Union (mIoU) for all the three datasets obtained by the different approaches. We achieve the best performance on all three datasets with a 14.8%, 10.0% and 7.7% relative improvement in mIoU over the source model on the GTA5 [23] \rightarrow Cityscapes [5] and SYNTHIA [24] \rightarrow Cityscapes and [18] \rightarrow SUN [28] respectively. This demonstrates how a light weight statistics update, which is applicable in the challenging SITA setting, could lead to a significant improvement in performance, with a minimal increase in inference time (Figure 3a).

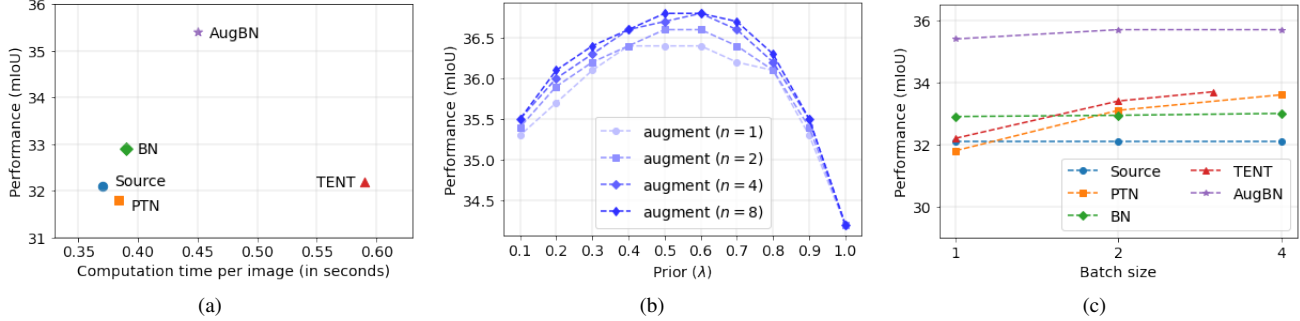


Figure 3. (a) Computation time vs Performance comparison (b) Performance of our algorithm for various augmentations and prior settings (c) Performance comparison for different batch sizes. TENT cannot fit batch size > 3 due to the high memory requirement of backprop. All these analyses are performed on SYNTHIA \rightarrow Cityscapes.

Table 2. Results for single image test-time adaptation for semantic segmentation. The first two columns are on outdoor scenes and the last column is on indoor dataset.

Methods	GTA5 → Cityscapes	SYNTHIA → Cityscapes	SceneNet → SUN
Source Model	37.6	32.1	26.5
PTN [20,27]	36.7	31.8	25.2
BN [27]	40.4	32.9	28.2
TENT [30]	37.1	32.2	25.7
AugBN	42.8	35.3	28.7

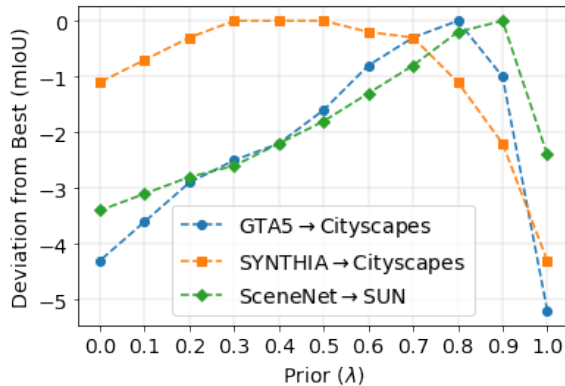


Figure 4. Performance of AugBN (relative to the maximum performance obtained) with varying λ . We used $\lambda = 0.8$ for all the segmentation experiments.

Computational Analysis The proposed method requires only one forward pass of the original test image itself along with its augmented versions, and thus the inference time is very close to the source model itself. We report the average computation time for all methods on the SYNTHIA [24] \rightarrow Cityscapes setting in Figure 3a. This computation time also includes the time required to compute the necessary aug-

mentations. Compared to TENT [30] which is currently the state-of-the-art TTA method, our method is 24% faster with a 9.6% relative improvement (Table 2) in performance. The speed of our method can be further improved by embedded implementations for better usage of GPUs. The simplicity of inference in the proposed method and its performance shows how universally applicable it is for any deployed application, as it conforms to the SITA setting.

Ablation of design choices. AugBN uses a combination of augmented samples around the current test image, and a prior factor λ to combine the source model's statistics to estimate the target statistics. Here, we analyse how the model performance varies with the choice of these parameters. Figure 11 shows the effect of the prior. $\lambda = 1$ uses only the source statistics, and hence is equivalent to the source model. $\lambda = 0$ on the other hand, ignores source statistics completely, and uses an aggregate of statistics from the single test image and its augmented samples. We observe that AugBN is strictly better than using the source model for all values of λ . Further, the results are not very sensitive to variations in λ , as 20% of the entire range of possible values gave results within 1 mIoU of the best result for all the three datasets. Note that we choose $\lambda = 0.8$ for all segmentation experiments.

Figure 3b shows a combination of changing prior λ and the number of augmented images on SYNTHIA \rightarrow Cityscapes. We can see with a higher number of augmented samples, the performance improves as it provides a more reliable estimate. Also, with the higher number of augmented samples, we observe a better stability over the prior λ . Though the focus of this work is on SITA setting where only a single test image is available for adaptation, AugBN can also be used for larger batch sizes. Figure 3c shows how performance of all the methods varies with different batch sizes on the SYNTHIA \rightarrow Cityscapes dataset. We observe that AugBN outperforms the other methods even for larger batch sizes. Since TENT requires backward propagation as well, it has a high memory requirement, and thus is not able

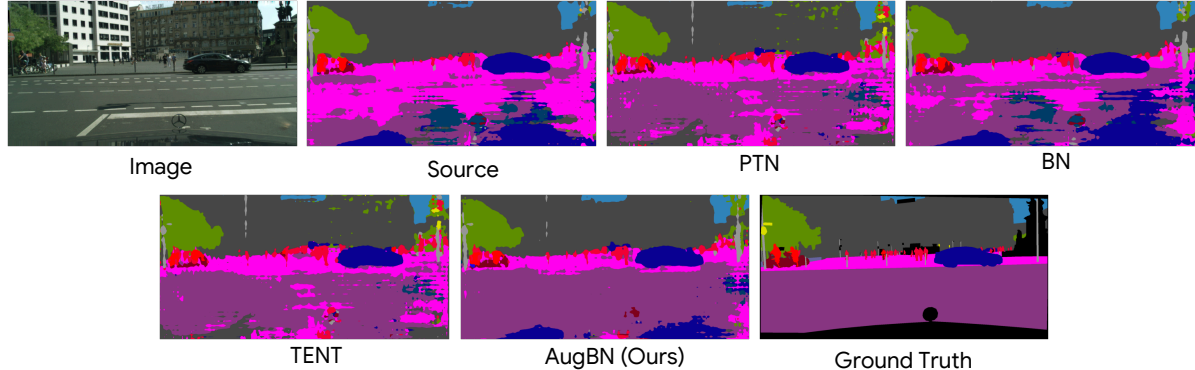


Figure 5. Visual comparison of the segmentation output using AugBN and the other methods.

to fit batch sizes more than 3, given the high dimensional inputs of size 512×1024 .

Qualitative Comparison. Figure 5 presents an example segmentation output for all the methods. We observe that the segmentation quality is much better in “AugBN” than “Source”, as the latter confuses road with sidewalk for large portions of the image, whereas after calibrating the batch-normalization statistics using AugBN, the predictions are significantly more aligned with the ground-truth. Also, compared to the other methods, AugBN appears closer to the ground truth.

4.2. Classification

Datasets and Implementation Details. We evaluate the AugBN method for the classification task on common adaptation datasets [19, 27, 29, 30], namely the corruption and perturbation data, CIFAR-10-C and ImageNet-C [8]. Following previous works, we report results on the highest severity level of corruption. For more details of the datasets, please refer to Appendix A. We compare the mean Classification Accuracy (mCA) over all 15 corruption types on both the datasets. We adopt the same network architecture used in the recent works [29, 30], i.e., ResNet-26 and ResNet-50 for CIFAR-10 and ImageNet respectively. The source model for CIFAR-10 is trained on one GPU with a batch size of 64, using SGD with cosine decay scheduler and an initial learning rate of 0.01. The source model achieves 93.84% accuracy on the CIFAR-10 test set. For ImageNet, the model is trained on 8x8 TPU slices with a batch size of 8192. We use Adam optimizer along with the cosine decay scheduler with an initial learning rate of 0.1. This source model obtains 76.4% accuracy on the ImageNet validation set. For ImageNet-C and CIFAR-10-C, we report results with prior $\lambda = 0.9$ and $\lambda = 0.7$ respectively. For all classification results, we use 4 augmented samples, each composed of 2 augmentations from color distortion [29], rotation, mirror reflection, Gaussian noise, vertical and horizontal flip augmentations, i.e., with $n = 4, k = 2, m = 6$ (Algorithm 2).

Table 3. Results on CIFAR10-C and ImageNet-C datasets. We report the mean Classification Accuracy (mCA) over all 15 corruptions of the highest severity (level 5).

Methods	CIFAR-10-C	ImageNet-C
Source	61.4	20.5
PTN [20, 27]	55.8	0.3
BN [27]	65.1	24.5
TENT [30]	55.9	0.3
AugBN	71.8	25.0

Baselines. We compare with strong state-of-the-art baselines, namely TENT [30], BN [27], and Prediction Time Normalization (PTN) [20]. Note that the results in the TENT paper [30] are for the online setting over a batch size of 64 and 128 for ImageNet-C and CIFAR-10-C respectively. For reproducing TENT numbers, we optimize the model for 5 iterations at test time with Adam optimizer with a learning rate of 0.001 as it gives the best results within our tested range of $[10^{-2}, 10^{-5}]$. For BN [27], we report results using their recommended parameter setting of $N = 16$.

Comparison with state-of-the-art. Table 3 shows that AugBN gives a huge 17% improvement on CIFAR-10-C compared to just using the source model directly, and also compares favourably with the state-of-the-art approaches. This justifies the effectiveness of the proposed framework for the SITA setting. The performance for every corruption is shown in Figure 7 for CIFAR-10-C. AugBN outperforms the baselines for majority of the corruption types. ImageNet-C is a much harder dataset to do adaptation using just a single instance, and the methods which do not incorporate source statistics (TENT [30] and PTN [20]) suffer a huge loss in performance as their normalisation statistics are highly incompatible with the source model. Meanwhile, BN [27] and AugBN which add a prior weight towards source statistics can handle adaptation using a single image better (Table 3).

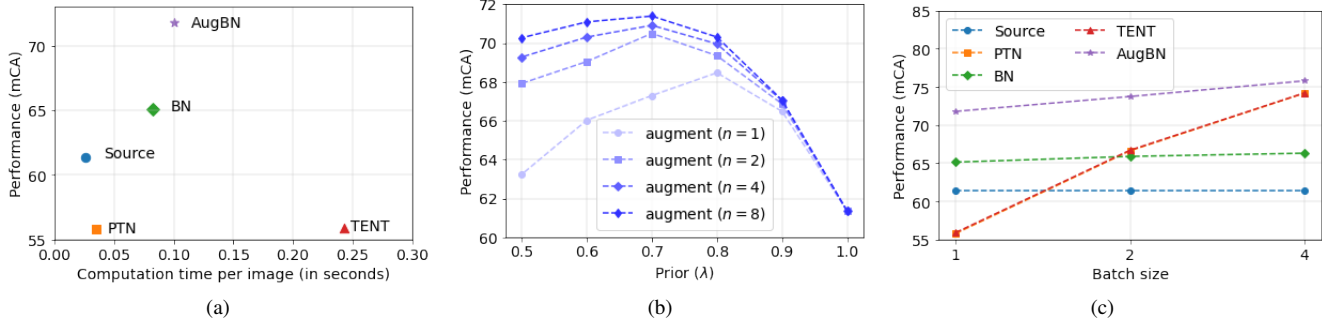


Figure 6. (a) Computation time vs performance comparison. (b) Performance of our algorithm for various augmentations and prior settings. (c) Performance comparison for different batch sizes. All these analysis are performed on CIFAR10-C dataset.

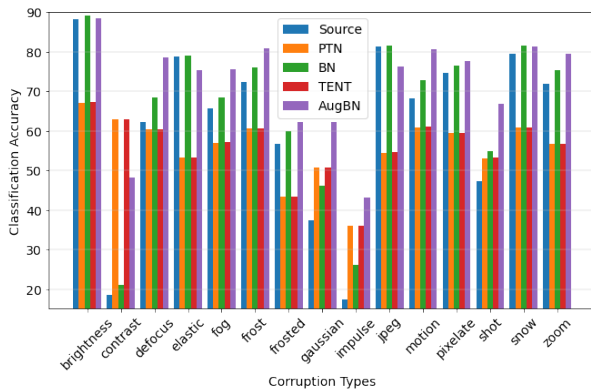


Figure 7. Performance comparison on CIFAR10-C corruptions.

Computational Analysis. Figure 6a reports the average computation time for all the methods on all the 15 corruption types of the CIFAR-10-C under the SITA setting. Similar to the segmentation case, this computation time includes the time required to compute the augmentations. Compared to TENT [30], the proposed method is 59% faster with a 28% improvement in mean Classification Accuracy (mCA).

Ablation of design choices. We analyse how the number of augmentations and prior weight (λ) affect the performance on the CIFAR-10-C dataset in Figure 6b. With an increase in the number of augmentations used, the performance improves. Moreover, it becomes more stable to changes in the prior (λ). The results follow the same trend as in the case of segmentation. We show additional results regarding the choice of prior (λ) in Appendix E. We further show the performance of our method on larger batch sizes on the CIFAR-10-C dataset in Figure 6c, where we still outperform other baselines. As expected, the performance of TENT improves consistently with larger batches.

5. Conclusion and Future Directions

In this work, we formalise the test time problem under the realistic and challenging Single Image Test-time Adaptation (SITA) setting. We propose AugBN framework which significantly outperforms the state-of-the-art while overcoming some of the limitations of the existing approaches. The strength of the proposed approach is in its simplicity and effectiveness for both semantic segmentation and classification applications.

Future Directions. In AugBN, the two main parametric choices are the augmentations and the prior. We observe that the results are stable for a wide range of choices and we keep them fixed for the entire dataset. However, all images may not need the same augmentations and prior, and it would be better to design a heuristic to choose them individually given the input image. We hypothesize that two factors can help to judiciously choose them - (i) the distance between the source statistics and the single image target statistics, and (ii) the stability of the target statistics to image perturbations/augmentations. This can be a very interesting direction for future works.

References

- [1] Alexander Bartler, Andreas Bühler, Felix Wiewel, Mario Döbler, and Binh Yang. Mt3: Meta test-time training for self-supervised test-time adaption. *CoRR*, abs/2103.16201, 2021. 3
- [2] Woong-Gi Chang, Tackgeun You, Seonguk Seo, Suha Kwak, and Bohyung Han. Domain-specific batch normalization for unsupervised domain adaptation. In *CVPR*, 2019. 4
- [3] Liang-Chieh Chen, George Papandreou, Iasonas Kokkinos, Kevin Murphy, and Alan L Yuille. Deeplab: Semantic image segmentation with deep convolutional nets, atrous convolution, and fully connected crfs. *TPAMI*, 2017. 5
- [4] Ting Chen, Simon Kornblith, Mohammad Norouzi, and Geoffrey Hinton. A simple framework for contrastive learning of visual representations. In *ICML*, 2020. 4

[5] Marius Cordts, Mohamed Omran, Sebastian Ramos, Timo Rehfeld, Markus Enzweiler, Rodrigo Benenson, Uwe Franke, Stefan Roth, and Bernt Schiele. The cityscapes dataset for semantic urban scene understanding. In *CVPR*, 2016. 5, 10

[6] Kaiming He, Xiangyu Zhang, Shaoqing Ren, and Jian Sun. Deep residual learning for image recognition. In *CVPR*, 2016. 5

[7] Dan Hendrycks and Thomas Dietterich. Benchmarking neural network robustness to common corruptions and perturbations. *ICLR*, 2019. 1

[8] Dan Hendrycks and Thomas Dietterich. Benchmarking neural network robustness to common corruptions and perturbations. *ICLR*, 2019. 2, 7

[9] Dan Hendrycks, Norman Mu, Ekin D Cubuk, Barret Zoph, Justin Gilmer, and Balaji Lakshminarayanan. Augmix: A simple data processing method to improve robustness and uncertainty. *ICLR*, 2020. 1

[10] Xuefeng Hu, M. Gökhan Uzunbas, Sirius Chen, Rui Wang, Ashish Shah, Ram Nevatia, and Ser-Nam Lim. Mixnorm: Test-time adaptation through online normalization estimation. *CoRR*, abs/2110.11478, 2021. 11

[11] S. Ioffe and C. Szegedy. Batch normalization: Accelerating deep network training by reducing internal covariate shift. In *ICML*, 2015. 4

[12] Neerav Karani, Ertunc Erdil, Krishna Chaitanya, and Ender Konukoglu. Test-time adaptable neural networks for robust medical image segmentation. *Medical Image Analysis*, 68:101907, 2021. 3

[13] Rui Li, Qianfen Jiao, Wenming Cao, Hau-San Wong, and Si Wu. Model adaptation: Unsupervised domain adaptation without source data. In *CVPR*, 2020. 2

[14] Yanghao Li, Naiyan Wang, Jianping Shi, Jiaying Liu, and Xiaodi Hou. Revisiting batch normalization for practical domain adaptation. *ICLRW*, 2017. 4

[15] Jian Liang, Dapeng Hu, and Jiashi Feng. Do we really need to access the source data? source hypothesis transfer for unsupervised domain adaptation. In *ICML*, 2020. 2

[16] Yuang Liu, Wei Zhang, and Jun Wang. Source-free domain adaptation for semantic segmentation. In *CVPR*, 2021. 2

[17] John McCormac, Ankur Handa, Stefan Leutenegger, and Andrew J Davison. Scenenet rgb-d: 5m photorealistic images of synthetic indoor trajectories with ground truth. *arXiv preprint arXiv:1612.05079*, 2016. 10

[18] John McCormac, Ankur Handa, Stefan Leutenegger, and Andrew J Davison. Scenenet rgb-d: Can 5m synthetic images beat generic imagenet pre-training on indoor segmentation? In *ICCV*, 2017. 5

[19] Chaithanya Kumar Mummadi, Robin Hutmacher, Kilian Rambach, Evgeny Levinkov, Thomas Brox, and Jan Hendrik Metzen. Test-time adaptation to distribution shift by confidence maximization and input transformation. *arXiv preprint arXiv:2106.14999*, 2021. 3, 7, 11

[20] Zachary Nado, Shreyas Padhy, D. Sculley, Alexander D’Amour, Balaji Lakshminarayanan, and Jasper Snoek. Evaluating prediction-time batch normalization for robustness under covariate shift. *CoRR*, 2020. 3, 5, 6, 7, 13, 14

[21] Fengchun Qiao, Long Zhao, and Xi Peng. Learning to learn single domain generalization. In *CVPR*, pages 12556–12565, 2020. 1

[22] Benjamin Recht, Rebecca Roelofs, Ludwig Schmidt, and Vaishaal Shankar. Do imagenet classifiers generalize to imagenet? In *ICML*, pages 5389–5400, 2019. 1

[23] Stephan R. Richter, Vibhav Vineet, Stefan Roth, and Vladlen Koltun. Playing for data: Ground truth from computer games. In *ECCV*, 2016. 5, 10

[24] German Ros, Laura Sellart, Joanna Materzynska, David Vazquez, and Antonio M. Lopez. The SYNTHIA Dataset: A large collection of synthetic images for semantic segmentation of urban scenes. In *CVPR*, 2016. 5, 6, 10

[25] Prabhu Teja S and Francois Fleuret. Uncertainty reduction for model adaptation in semantic segmentation. In *CVPR*, 2021. 2

[26] Shiori Sagawa, Pang Wei Koh, Tatsunori B Hashimoto, and Percy Liang. Distributionally robust neural networks for group shifts: On the importance of regularization for worst-case generalization. *ICLR*, 2020. 1

[27] Steffen Schneider, Evgenia Rusak, Luisa Eck, Oliver Bringmann, Wieland Brendel, and Matthias Bethge. Improving robustness against common corruptions by covariate shift adaptation. In *NeurIPS*, 2020. 3, 4, 5, 6, 7, 11, 13, 14

[28] Shuran Song, Samuel P Lichtenberg, and Jianxiong Xiao. Sun rgb-d: A rgb-d scene understanding benchmark suite. In *CVPR*, 2015. 5, 10

[29] Yu Sun, Xiaolong Wang, Zhuang Liu, John Miller, Alexei A. Efros, and Moritz Hardt. Test-time training with self-supervision for generalization under distribution shifts. In *ICML*, 2020. 1, 2, 3, 7, 10, 11

[30] Dequan Wang, Evan Shelhamer, Shaoteng Liu, Bruno Olshausen, and Trevor Darrell. Tent: Fully test-time adaptation by entropy minimization. In *ICLR*, 2021. 1, 2, 3, 4, 5, 6, 7, 8, 10, 11, 13, 14

[31] Colin Wei, Kendrick Shen, Yining Chen, and Tengyu Ma. Theoretical analysis of self-training with deep networks on unlabeled data. *ICLR*, 2021. 4

[32] Hao-Wei Yeh, Baoyao Yang, Pong C Yuen, and Tatsuya Harada. Sofa: Source-data-free feature alignment for unsupervised domain adaptation. In *WACV*, 2021. 2

[33] Fuming You, Jingjing Li, and Zhou Zhao. Test-time batch statistics calibration for covariate shift. *CoRR*, abs/2110.04065, 2021. 11

[34] Marvin Zhang, Sergey Levine, and Chelsea Finn. MEMO: test time robustness via adaptation and augmentation. *CoRR*, abs/2110.09506, 2021. 11

Appendix A. Datasets

A.1. Semantic Segmentation

GTA5 → Cityscapes: In this setting, we consider GTA5 [23] as the source and Cityscapes [5] as the target dataset. The source images are at 760×1280 resolution, while the target images are used at 512×1024 . The datasets have 19 categories. The source dataset (GTA5) has 24966 training images. We perform test time adaptation on the validation set which has 500 images of Cityscapes.

SYNTHIA → Cityscapes: In this setting, we consider SYNTHIA [24] as the source and Cityscapes [5] as the target dataset. SYNTHIA contains 9400 training images. However, unlike GTA5, due to lack of proper annotations for a few categories in SYNTHIA, we remove them from evaluation and report the results for 16 categories, following the literature. The validation set used for test-time adaptation is again the 500 images commonly used for Cityscapes evaluation.

SceneNet → SUN: Both of the above two settings are for outdoor scenes, and in this setting we consider indoor scenes with SceneNet [17] as the source and SUN [28] as the target. The SceneNet dataset has around 5 million simulated images. However, a lot of the images are rather simple with only a few categories in them. Thus, to train the source model, we only choose the top 50,000 images having the highest number of categories of SceneNet. For test-time adaptation, we perform experiments on the test set of SUN containing 5050 images. Both of these datasets contain 13 categories. Specifically, we use the label transformation available with the SceneNet dataset¹ to map the labels in the SUN dataset such that it matches with the label space of SceneNet.

A.2. Classification

ImageNet-C: The ImageNet-C dataset consists of perturbed and corrupted versions of the ImageNet validation set images. The ImageNet-C data consists of 15 different modes of corruption which are shown in Figure 8. These corruptions are algorithmically generated from 4 broad categories – *noise, blur, weather* and *digital*. Each type of corruption has 5 levels of severity, resulting in 75 distinct corruptions. These corruption types at different severity levels simulate a wide variety of challenging and realistic test time distribution shifts. Each corruption set has 50000 test images, which are at 224×224 resolution. For the results in the paper, we report the mean Classification Accuracy on all 15 corruptions of the highest severity level (level 5), with results for other severity levels available in this appendix.

CIFAR-10-C: The CIFAR-10-C dataset consists of perturbed and corrupted versions of the CIFAR-10 test set images. The CIFAR-10-C data consists of 15 different modes



Figure 8. 15 Corruption types for the ImageNet-C dataset. All corruptions are shown at severity level 3.

of corruption, which are the same as in the ImageNet-C case. Similar to ImageNet-C, each of the corruption types has 5 different levels of severity, resulting in 75 distinct corruptions. Each corruption test set consists of 10000 images, which are at 32×32 resolution. For the results in the paper (Table 3), we report the mean Classification Accuracy on all 15 corruptions of the highest severity level (level 5), as is done in other recent works [29,30]. Results for other severity levels are available in this appendix.

Appendix B. Results at all severity levels

CIFAR-10-C: We show classification accuracy for all 5 severity levels, for each of the 15 corruption types for all the methods, in Table 4-8. At lower corruption levels, the performance of the source model itself is very good, as the source distribution is close to the test distribution. We do not tune the augmentations for different corruption levels. Emphasis given to the augmented samples can be controlled by the prior (λ). We use $\lambda = 0.9$ for severity levels 1-3, and $\lambda = 0.7$ for higher severity levels. AugBN provides significant gains in performance over the source model in all cases, especially at high severity level corruptions (Table 8).

ImageNet-C: We show classification accuracy for all 5 severity levels, for each of the 15 corruption types for all the methods, in Table 9-13. At lower corruption levels, the prior (λ) needs to have more emphasis on the source statistics. We use $\lambda = 0.95$ for severity levels 1 and 2, and use $\lambda = 0.9$ for the remaining cases. AugBN provides significant gains in performance over the source model, especially at high severity level corruptions (Table 13).

¹<https://github.com/ankurhanda/sunrgbd-meta-data>

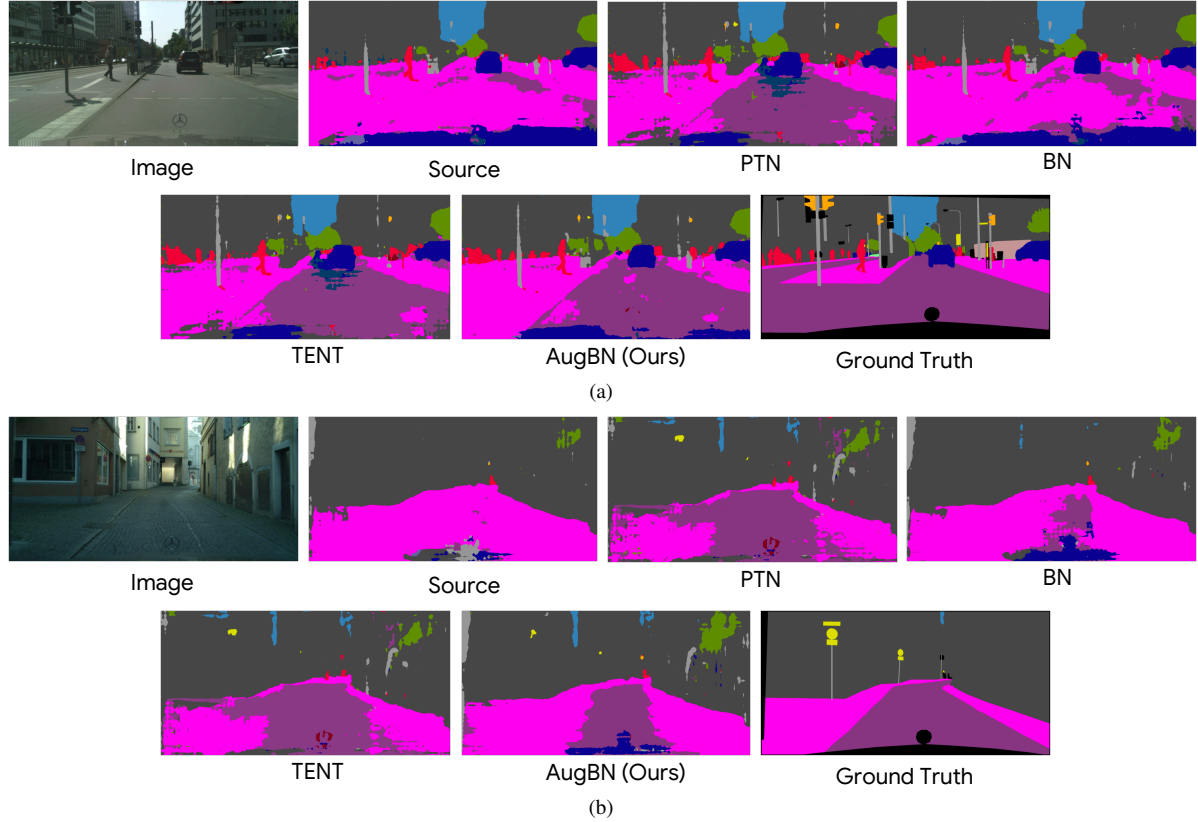


Figure 9. Additional qualitative results for the Semantic Segmentation task.

Appendix C. Qualitative Results

Figure 9 presents two additional examples of the segmentation outputs for all the methods. We observe that the segmentation quality is much better in “AugBN” than “Source”, as the latter confuses road with sidewalk for large portions of the image in both (a) and (b), whereas after calibrating the batch-normalization statistics using AugBN, the predictions are significantly more aligned with the ground-truth. In Figure 9a the persons and cars are better defined in AugBN results when compared to other methods.

Appendix D. Augmentations

We show the various augmentations $\{a_1, \dots, a_m\}$ from which augmented samples can be generated for the AugBN algorithm in Figure 10. Out of these augmentations, we randomly pick $k(\leq m)$ augmentations and use them as described in Algorithm 2 in the paper.

Appendix E. Choice of prior

All test time adaptation methods [10, 19, 27, 29, 30, 33, 34] rely on hyper-parameters which are picked beforehand and used during the adaptation process. While we do not expect a

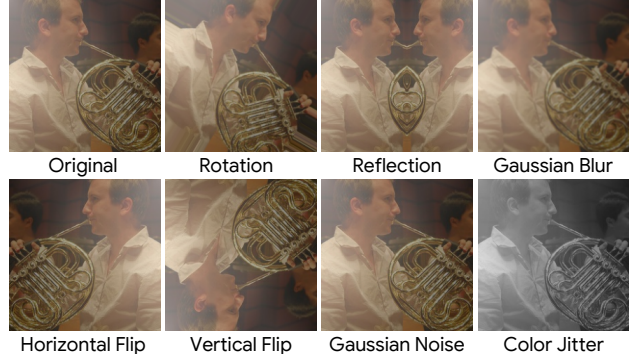


Figure 10. Illustration of augmentations used to create a batch with augmented samples.

holdout or validation set to tune adaptation parameters in the realistic test time adaptation setting, these can be used if they are available. ImageNet-C and CIFAR-10-C datasets have 4 holdout corruption sets - *Spatter*, *speckle noise*, *saturate* and *Gaussian blur*. The method can be evaluated on these holdout sets to get a reasonable indication of which range of λ values which can work well in practice. For CIFAR-10-C, the best mCA of 74.9 is obtained at $\lambda = 0.7$, and remains

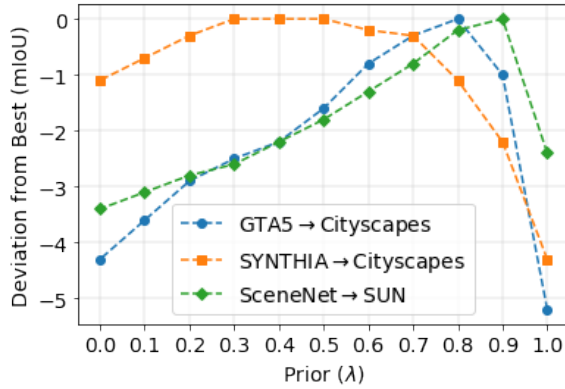


Figure 11. Performance of AugBN (relative to the maximum performance obtained) with varying λ . We used $\lambda = 0.8$ for all the segmentation experiments.

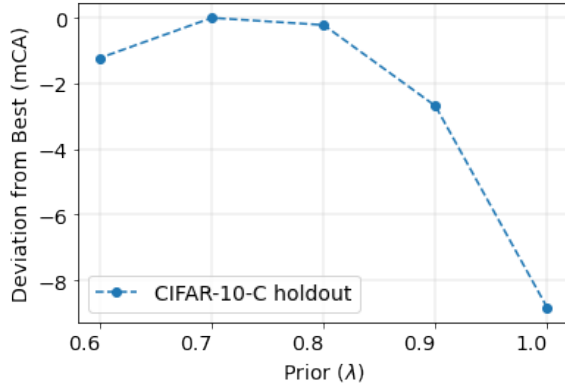


Figure 12. Performance of AugBN (relative to the maximum performance obtained) with varying λ on the CIFAR-10-C holdout corruptions. We used $\lambda = 0.7$ for the CIFAR-10-C classification results in the paper (Table 3).

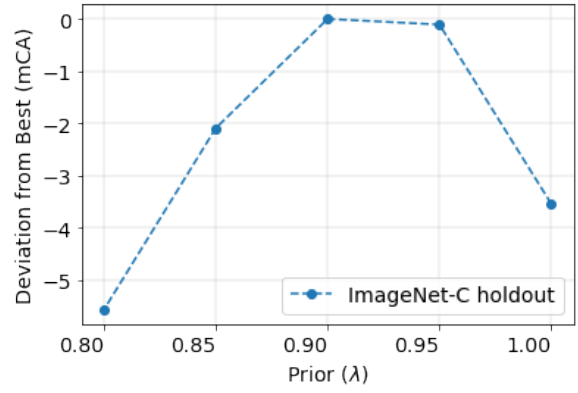


Figure 13. Performance of AugBN (relative to the maximum performance obtained) with varying λ on the CIFAR-10-C holdout corruptions. We used $\lambda = 0.9$ for the ImageNet-C classification results in the paper (Table 3).

stable for $\sim 20\%$ of the prior range, as shown in Figure 12. For ImageNet-C, the best mCA of 31.8 is at $\lambda = 0.9$, and the deviation from the best result at different priors (λ) is shown in Figure 13. We use these prior values for the results in the paper. However, in the case of segmentation, there are no holdout sets, so we use a fixed prior $\lambda = 0.8$ for all datasets, even when better results were available at other λ values. For example, in Figure 11, $\lambda = 0.9$ produces a better result for the SceneNet \rightarrow SUN and $\lambda = 0.3$ perform the best for SYNTHIA \rightarrow Cityscapes, but we still report results with $\lambda = 0.8$ in the paper, being consistent with the spirit of test time adaptation. Further, these results demonstrate that the results are not very sensitive with respect to the exact choice of λ . In the future extension of this work, an algorithm can be developed to automatically find the appropriate prior weight (λ) based on the test sample.

Table 4. Results for CIFAR-10-C dataset, with severity level 1 corruptions.

Method	brightness	contrast	defocus blur	elastic	fog	frost	frosted glass blur	gaussian noise	impulse noise	jpeg compression	motion blur	pixelate	shot noise	snow	zoom blur	mCA
Source	93.1	92.1	93.2	89.3	92.7	91.1	65.5	87.4	78.5	89.9	90.0	92.2	90.3	88.6	87.5	88.1
PTN [20,27]	69.6	69.6	69.5	65.0	69.7	67.9	50.6	65.4	57.8	63.8	67.5	68.1	67.6	63.9	65.8	65.5
BN [27]	93.4	92.5	93.2	89.7	92.9	91.6	69.2	88.6	80.6	90.1	90.7	92.4	90.8	88.9	88.3	88.9
TENT [30]	69.9	69.8	69.5	65.2	69.7	68.3	50.5	65.6	58.1	63.9	67.5	68.3	67.8	64.0	65.8	65.6
AugBN	93.2	92.7	93.0	89.6	92.7	91.6	71.0	88.9	80.8	90.0	90.9	92.2	91.0	88.7	88.7	89.0

Table 5. Results for CIFAR-10-C dataset, with severity level 2 corruptions.

Method	brightness	contrast	defocus blur	elastic	fog	frost	frosted glass blur	gaussian noise	impulse noise	jpeg compression	motion blur	pixelate	shot noise	snow	zoom blur	mCA
Source	92.6	86.3	91.7	89.3	90.9	87.5	66.8	74.0	65.0	86.2	84.4	91.1	86.0	82.5	86.0	84.0
PTN [20,27]	69.4	69.7	68.9	64.4	68.4	66.4	51.5	60.8	51.8	60.0	65.9	66.6	64.8	60.3	64.7	63.6
BN [27]	92.9	88.1	91.9	89.5	91.4	88.4	70.2	77.8	68.7	86.6	86.2	91.1	87.4	83.8	87.3	85.4
TENT [30]	69.7	69.6	69.1	64.5	68.5	66.6	51.5	61.1	51.6	60.0	65.8	66.8	64.9	60.5	64.8	63.7
AugBN	92.2	90.0	91.1	88.8	91.0	88.7	72.5	82.3	70.1	85.2	87.3	90.1	88.2	84.3	87.5	85.9

Table 6. Results for CIFAR-10-C dataset, with severity level 3 corruptions.

Method	brightness	contrast	defocus blur	elastic	fog	frost	frosted glass blur	gaussian noise	impulse noise	jpeg compression	motion blur	pixelate	shot noise	snow	zoom blur	mCA
Source	91.9	78.4	88.3	86.8	87.9	81.3	72.4	55.6	54.0	85.3	76.7	90.2	69.6	83.1	82.4	78.9
PTN [20,27]	69.1	69.0	67.9	63.0	67.1	63.6	52.5	56.3	47.0	58.5	63.4	65.7	59.5	60.3	62.5	61.7
BN [27]	92.2	82.0	89.3	87.3	88.8	83.4	74.1	62.5	59.8	85.7	80.3	90.5	73.7	84.1	84.3	81.2
TENT [30]	69.2	69.1	67.9	63.2	67.1	63.7	52.6	56.3	47.0	58.7	63.4	65.8	59.6	60.5	62.5	61.8
AugBN	92.3	83.9	89.4	87.4	89.2	84.7	75.3	67.1	61.4	85.3	81.5	90.4	76.1	84.2	84.7	82.2

Table 7. Results for CIFAR-10-C dataset, with severity level 4 corruptions.

Method	brightness	contrast	defocus blur	elastic	fog	frost	frosted glass blur	gaussian noise	impulse noise	jpeg compression	motion blur	pixelate	shot noise	snow	zoom blur	mCA
Source	91.1	61.5	81.6	82.3	82.7	80.6	51.6	45.5	30.4	83.4	76.3	85.6	61.1	81.7	78.8	71.6
PTN [20,27]	68.7	68.2	65.3	57.8	64.0	62.9	43.7	53.2	39.8	56.5	63.2	64.2	56.8	59.4	60.4	58.9
BN [27]	91.4	68.1	83.8	83.3	84.5	83.3	56.2	54.0	41.6	83.8	79.8	86.5	66.6	82.5	81.3	75.1
TENT [30]	69.0	68.0	65.5	58.0	64.1	63.2	43.6	53.5	39.9	56.6	63.4	64.4	57.0	59.5	60.5	59.1
AugBN	89.6	82.8	84.9	79.9	84.8	84.7	60.2	68.2	53.0	79.3	82.9	85.2	75.1	79.9	82.1	78.2

Table 8. Results for CIFAR-10-C dataset, with severity level 5 corruptions.

Method	brightness	contrast	defocus blur	elastic	fog	frost	frosted glass blur	gaussian noise	impulse noise	jpeg compression	motion blur	pixelate	shot noise	snow	zoom blur	mCA
Source	88.3	18.5	62.2	78.8	65.7	72.5	56.8	37.4	17.5	81.3	68.2	74.6	47.3	79.5	72.0	61.4
PTN [20,27]	67.2	63.0	60.4	53.3	57.0	60.6	43.3	50.7	36.0	54.5	61.0	59.4	53.0	60.8	56.7	55.8
BN [27]	89.2	21.1	68.4	79.1	68.4	76.0	60.0	46.1	26.1	81.5	72.9	76.6	55.0	81.5	75.4	65.1
TENT [30]	67.2	63.0	60.4	53.3	57.1	60.6	43.3	50.8	36.1	54.6	61.1	59.5	53.2	60.9	56.6	55.8
AugBN	88.5	48.2	78.5	75.3	75.5	81.0	62.2	62.3	43.1	76.3	80.6	77.8	66.8	81.2	79.4	71.8

Table 9. Results for ImageNet-C dataset, with severity level 1 corruptions.

Method	brightness	contrast	defocus blur	elastic transform	fog	frost	glass blur	gaussian noise	impulse noise	jpeg compression	motion blur	pixelate	shot noise	snow	zoom blur	mCA
Source	73.9	66.0	58.2	68.2	65.5	62.2	54.8	65.0	55.6	65.5	64.6	58.8	63.6	55.5	52.2	62.0
PTN [20,27]	1.0	0.9	0.4	0.7	0.8	0.7	0.5	0.7	0.6	0.7	0.8	0.6	0.7	0.6	0.5	0.7
BN [27]	73.6	68.0	60.6	69.0	66.4	63.0	58.1	64.5	57.2	65.3	66.7	61.3	62.9	59.6	54.1	63.4
TENT [30]	0.9	0.9	0.4	0.7	0.7	0.7	0.5	0.7	0.6	0.7	0.8	0.6	0.8	0.6	0.5	0.7
AugBN	73.5	67.7	60.2	68.6	66.0	62.5	57.4	64.8	56.8	64.8	66.1	60.5	62.9	58.9	53.6	63.0

Table 10. Results for ImageNet-C dataset, with severity level 2 corruptions.

Method	brightness	contrast	defocus blur	elastic transform	fog	frost	glass blur	gaussian noise	impulse noise	jpeg compression	motion blur	pixelate	shot noise	snow	zoom blur	mCA
Source	72.2	60.1	50.6	47.5	61.3	46.6	41.1	56.4	46.8	62.3	49.7	62.0	52.9	32.3	41.8	52.2
PTN [20,27]	0.9	0.8	0.3	0.4	0.7	0.5	0.3	0.6	0.5	0.6	0.5	0.7	0.6	0.4	0.4	0.5
BN [27]	72.0	63.2	53.3	49.1	63.3	49.5	45.6	55.8	47.9	61.8	56.5	63.6	52.0	41.9	44.1	54.6
TENT [30]	0.9	0.8	0.4	0.4	0.7	0.5	0.3	0.6	0.5	0.6	0.5	0.6	0.6	0.4	0.4	0.5
AugBN	72.0	63.2	53.4	48.9	63.2	49.4	45.4	56.0	48.0	61.5	56.1	63.3	52.1	41.6	44.2	54.6

Table 11. Results for ImageNet-C dataset, with severity level 3 corruptions.

Method	brightness	contrast	defocus blur	elastic transform	fog	frost	glass blur	gaussian noise	impulse noise	jpeg compression	motion blur	pixelate	shot noise	snow	zoom blur	mCA
Source	69.3	47.8	36.4	55.4	55.8	35.2	17.8	41.3	38.5	60.0	28.2	47.7	38.7	36.0	35.4	42.9
PTN [20,27]	0.8	0.7	0.3	0.5	0.6	0.3	0.2	0.5	0.4	0.5	0.4	0.5	0.5	0.4	0.3	0.5
BN [27]	69.2	45.8	35.9	55.4	55.2	34.2	17.6	41.4	38.6	59.8	29.1	47.6	38.9	36.4	35.5	42.7
TENT [30]	0.8	0.7	0.3	0.5	0.6	0.3	0.2	0.5	0.4	0.5	0.4	0.5	0.5	0.4	0.3	0.5
AugBN	67.2	55.6	36.9	58.0	57.9	40.2	24.4	39.6	39.0	56.6	39.6	48.4	37.9	45.1	36.8	45.5

Table 12. Results for ImageNet-C dataset, with severity level 4 corruptions.

Method	brightness	contrast	defocus blur	elastic transform	fog	frost	glass blur	gaussian noise	impulse noise	jpeg compression	motion blur	pixelate	shot noise	snow	zoom blur	mCA
Source	64.9	22.7	25.4	41.1	53.4	33.0	12.7	23.0	20.2	51.7	12.4	31.1	18.4	25.1	28.6	30.9
PTN [20,27]	0.7	0.4	0.2	0.4	0.6	0.4	0.2	0.3	0.3	0.4	0.3	0.3	0.3	0.3	0.3	0.4
BN [27]	65.3	30.8	27.7	47.6	56.0	37.6	17.0	24.4	22.7	50.4	23.2	34.1	20.4	34.7	31.2	34.9
TENT [30]	0.7	0.4	0.2	0.4	0.6	0.4	0.2	0.3	0.3	0.4	0.2	0.4	0.3	0.3	0.3	0.4
AugBN	63.5	35.8	26.0	48.6	55.2	38.7	18.3	24.3	23.4	47.4	24.5	32.8	20.8	35.5	30.5	35.0

Table 13. Results for ImageNet-C dataset, with severity level 5 corruptions.

Method	brightness	contrast	defocus blur	elastic transform	fog	frost	glass blur	gaussian noise	impulse noise	jpeg compression	motion blur	pixelate	shot noise	snow	zoom blur	mCA
Source	58.2	5.8	17.2	15.5	42.9	26.4	8.7	7.3	7.3	39.7	7.2	20.8	8.8	18.8	22.8	20.5
PTN [20,27]	0.6	0.2	0.2	0.2	0.5	0.3	0.1	0.2	0.2	0.2	0.2	0.3	0.3	0.3	0.2	0.3
BN [27]	59.5	10.8	19.1	24.7	46.7	31.5	11.9	9.3	9.9	38.9	15.5	24.8	11.5	28.2	25.0	24.5
TENT [30]	0.6	0.3	0.2	0.2	0.4	0.3	0.1	0.2	0.2	0.3	0.2	0.3	0.3	0.3	0.2	0.3
AugBN	58.1	13.8	17.8	28.2	46.8	32.9	12.6	10.4	11.1	35.4	17.6	23.3	12.4	30.1	24.9	25.0